

Development of Robust Safety-of-Life Navigation Receivers

Marcos V. T. Heckler, *Member, IEEE*, Manuel Cuntz, Andriy Konovaltsev, Lukasz A. Greda, *Member, IEEE*, Achim Dreher, *Senior Member, IEEE*, and Michael Meurer, *Senior Member, IEEE*

Abstract—This paper summarizes the development of safety-of-life receivers for global navigation satellite systems. Two receiver systems have been successfully fabricated, integrated, and tested by means of field experiments. Implementation issues of these two systems are described in this paper. The third generation of this receiving system is based on a dual-band approach with antennas that are able to separate two frequency bands using two outputs. Measured results show that high isolation between the two bands can be achieved.

Index Terms—Global navigation satellite systems (GNSSs), navigation systems, safety-of-life (SoL) navigation receivers.

I. INTRODUCTION

THE NUMBER of applications that rely on satellite navigation systems has increased dramatically in the last two decades. Future navigation systems will require more precise and reliable receivers to offer safety-of-life (SoL) services. In order to carry out research on the implementation and improvement of existing algorithms, the German Aerospace Center (DLR), Institute of Communications and Navigation, Wessling, Germany, has started the continuous development of demonstration systems. These are dedicated to process signals from the existing American Global Positioning System (GPS) and the future European Galileo navigation system.

In order to comply with the requirements that receivers for SoL applications have to fulfill, the system robustness is a critical issue. Out-of-band interferers may be suppressed by using filters that present enough attenuation outside the bands of interest. However, in-band interference may be the issue. To minimize this problem, the implementation of the designed receivers foresees the application of antenna arrays, which allow using digital beamforming (DBF) techniques to suppress interference and multipath, in contrast to conventional receivers, which are

Manuscript received October 29, 2010; accepted November 29, 2010. Date of publication February 04, 2011; date of current version April 08, 2011. This paper is an expanded paper from the IEEE MTT-S International Microwave Symposium, May 23–28, 2010, Anaheim, CA.

M. V. T. Heckler was with the German Aerospace Center (DLR), Institute of Communications and Navigation, 82234 Wessling, Germany. He is now with the Alegrete Center of Technology, Universidade Federal do Pampa, 97546-550 Alegrete RS, Brazil (e-mail: marcos.heckler@dlr.de).

M. Cuntz, A. Konovaltsev, L. A. Greda, A. Dreher, and M. Meurer are with the German Aerospace Center (DLR), Institute of Communications and Navigation, 82234 Wessling, Germany (e-mail: manuel.cuntz@dlr.de; andriy.konovaltsev@dlr.de; lukasz.greda@dlr.de; achim.dreher@dlr.de; michael.meurer@dlr.de).

Color versions of one or more of the figures in this paper are available online at <http://ieeexplore.ieee.org>.

Digital Object Identifier 10.1109/TMTT.2010.2103090



Fig. 1. Broadband 2×2 array.

normally based on a single-antenna architecture. Moreover, by applying the correct weighting coefficients, derived from adaptive beamforming algorithms, an improvement of the gain in the direction of arrival (DoA) of the GNSS signals can be achieved, thus improving the signal-to-interference ratio [1].

Highly robust dual-band operation requires novel concepts, which are presented in this paper. The first part of the paper briefly describes the first demonstrator, which was based on a broadband antenna approach. The second part presents the architecture of a single-band demonstrator operating in the L1 band (1568–1582 MHz), as well as results obtained by field tests. The third part of this contribution shows the trends of the new development, which operates in dual-band mode in the E5a/E5b (1164–1215 MHz) and E1 bands (1559–1591 MHz).

II. RECEIVER WITH A BROADBAND ANTENNA ARRAY

In the first version of the demonstrator, the antennas were designed to cover the whole band from 1.15 to 1.60 GHz in which the Galileo signals E1, E5, and E6 are allocated. The antenna presented a broadband impedance matching and the frequency selectivity was determined only by the front ends and after one pre-amplification. The microstrip antenna was composed of a circular main patch that was fed by four circular plates mounted below and capacitively coupled to the main radiator [2]–[4]. The capacitive effect also compensates the inductive component introduced by the long vias connecting the disks to the antenna feeding system. This was necessary because the broadband impedance matching could only be obtained by employing a thick substrate. Broadband circular polarization operation was achieved by a feeding system that was composed of two 90° and

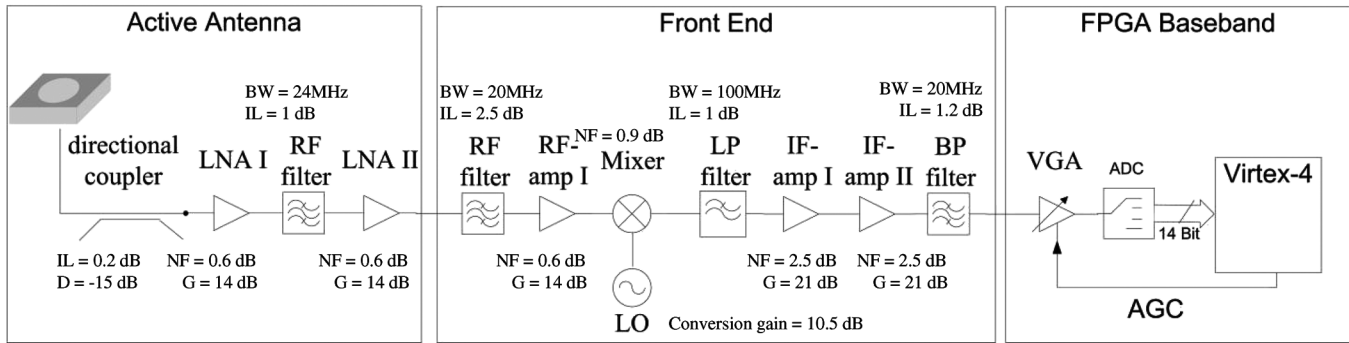


Fig. 2. Block diagram of receiver architecture.

one 180° hybrid so that the fields at each of the four feeding disks presented 90° phase shift one from another, thus providing a sequentially rotated feeding scheme.

The demonstrator is shown in Fig. 1, where one antenna has been removed to show the complexity of the feeding system below each element. The main advantages of this demonstrator were the operability in the entire band of interest for GNSS systems operating in L band and good axial ratio performance in the whole desired band. One drawback was the difficulty of calibrating this antenna array properly since the antenna feeding system is not part of the calibration signal path and the total phase delay of each channel could not be completely determined. Another problem was low robustness against out-of-band interference since the antenna presented broadband characteristic and no additional filtering has been foreseen before the first low-noise amplifier (LNA). The resulting array volume was about 190 mm × 190 mm × 100 mm. The relatively big height of the antenna was caused mainly due to low level of integration of its architecture.

III. SINGLE-BAND (L1) RECEIVER

The broadband array allowed testing beamforming algorithms and DoA estimators, which have been initially implemented to operate in the L1 band. Since robustness can be strongly increased if only the L1 band is targeted during the design of the hardware, a second generation of the receiver has been developed and implemented. The receiver architecture is shown in Fig. 2. Each part of it will be detailed below.

A. Antenna Array

The antenna has been implemented in microstrip technology by employing an off-center dual-feed scheme [5]. To obtain circular polarization operation, the two feeding lines are connected by a 90° hybrid. The antenna has been optimized to present broad radiation pattern and moderate suppression of out-of-band interference. For instance, GSM signals at 1.7–1.8 GHz may drive the whole receiver into saturation if no proper filtering is achieved already in the first stage. In this range, the gain of the passive antenna in the boresight is at least 14 dB below its in-band value.

The passive antenna is directly connected with an RF-board containing two LNAs and one passband filter, as schematically shown in Fig. 3. The connection is made by means of a coaxial transition of the SMP type. This architecture has been preferred

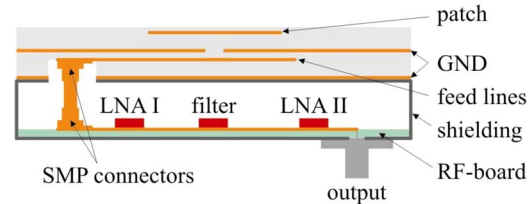


Fig. 3. Schematic cross-sectional view of the connection between the microstrip antennas and the microwave components.

instead of integrating the components directly into the antenna structure for the purpose of allowing the replacement of faulty LNAs without the risk of possible damage to the passive array. After the integration of the LNAs and the bandpass filter, the suppression in the aforementioned GSM band was improved to over 40 dB.

This antenna element has been used to compose the 2 × 2 array that is schematically shown in Fig. 4, where the patches are shown by dashed black lines, the slots by solid black lines, and the feed lines by red lines (in online version). Since calibration is an important issue for systems based on DBF techniques, a power divider has been integrated into the array structure in the same layer as the feed lines and the 90° hybrids. In order to distribute the calibration signal, directional couplers have been placed at the outputs of each of the four passive antennas. The four RF boards located below the array elements are shielded from each other and from the external environment by means of a metallic box so as to prevent crosstalk between the four channels. The isolation between the channels has been measured and values better than 40 dB have been obtained.

This array allows scanning the main beam down to 42° from boresight. The built prototype is shown in Fig. 5. While the length and width were the same as for the broadband array, the total height of the single-band array could be reduced to approximately 3 cm.

B. Front Ends

The front ends for further amplification and down conversion are physically separated from the antenna array. They present the configuration shown in the block diagram of Fig. 2. The front end provides about 60 dB of amplification, which is obtained using three amplifying stages (one RF and two IF stages), plus down conversion, where the RF central frequency (1575 MHz)

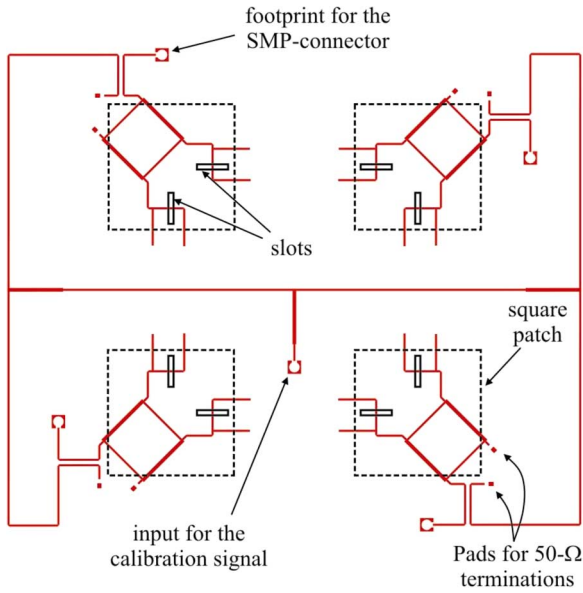


Fig. 4. Schematic view of the 2 × 2 array.



Fig. 5. Single-band (L1) 2 × 2 microstrip array during the field tests.

is converted to 78 MHz. Fig. 6 shows a photograph of four implemented channels. By considering the values of insertion loss, gain, and noise figure given in Fig. 2, one can calculate the noise figure of the whole chain. By applying the Friis’ equation, the resulting noise figure for the receiver is estimated to be approximately 0.9 dB.

Out-of-band interference is a critical point for SoL receivers. For this reason, it is important to assess the maximum power allowed to enter into the receiver chain as a function of frequency so as to prevent the amplifiers to operate under saturation. This assessment has been done by considering the gain and the 1-dB compression point ($P_{out1\text{ dB}}$) of each amplifier. The $P_{out1\text{ dB}}$ of the first three amplifiers in the receiver chain is 21 dBm and for the last two it is 20.5 dBm. Since the aimed application for this receiver is in the field of civil aviation, the receiver is designed to fulfill the high demands on robustness. References [6] and [7] state the maximum interference power levels at the receiver antenna. These power levels are frequency dependent

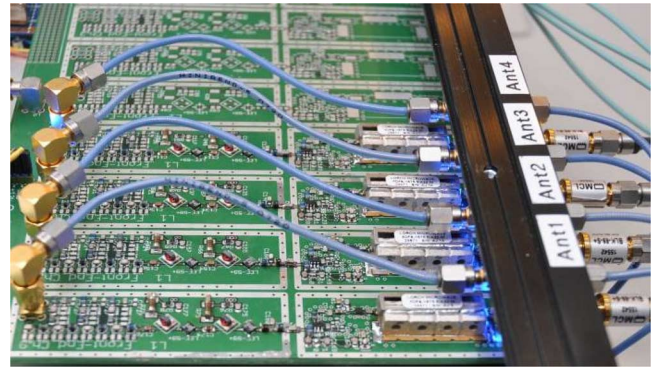


Fig. 6. Front ends implemented for the reception of E1.

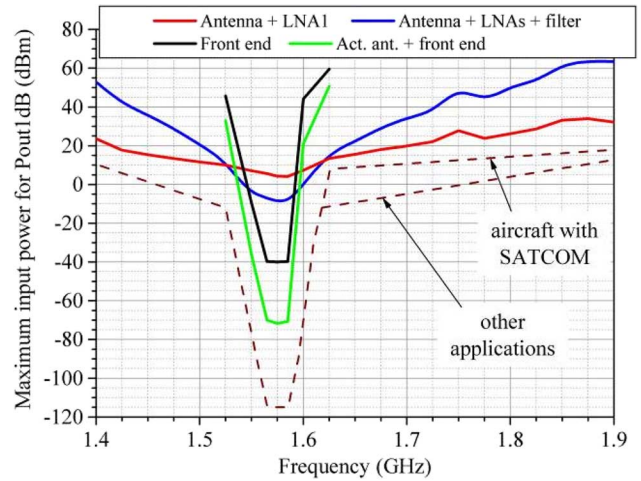


Fig. 7. Maximum allowed input power including the different parts of the receiver.

and are shown via the dashed lines in Fig. 7. Knowing the maximum interference power at the input of the antenna, the output power of each receiver stage can be computed. Due to the filters, the power of out-of-band interference can be higher than for in-band interference. Fig. 7 shows for several receiver stages the input power over frequency that drives the amplifiers to the 1-dB compression point. It can be seen that for the first LNA, out-of-band interference has the highest potential of saturation, whereas the last amplifier can only be saturated by in-band interference. It can be seen in Fig. 7 that for the interference levels specified in [6] and [7], the receiver chain will not be saturated because all curves are well above the dashed line. The requirements were fulfilled by the single-band receiver thanks to the frequency selective antenna property, along with the concept of using an LNA with moderate gain (14 dB) between the array elements and the passband filters with 24-MHz bandwidth.

C. Field-Programmable Gate Array (FPGA)/Digital Module

The FPGA/digital module consists of a Lyrtech VHS-ADC board and an embedded PC. The VHS board contains 16 ADC channels, a Virtex4-SX55 FPGA, and a PXI interface. The FPGA module comprises mainly three tasks: down conversion to baseband, data reduction, and data recording.

The IF signals of the front ends are centered around 78 MHz with a bandwidth of 14 MHz. These signals are digitized by four

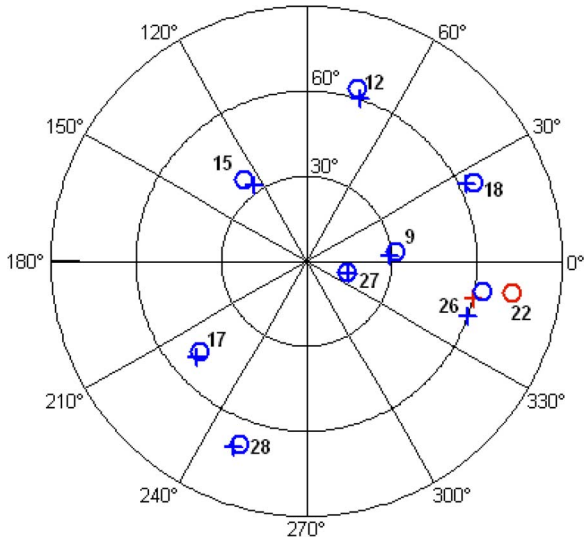


Fig. 8. Results of the DoA estimation. The circles denote true DoAs of GPS satellite signals and the crosses show the time-averaged estimations obtained by the DoA algorithm.

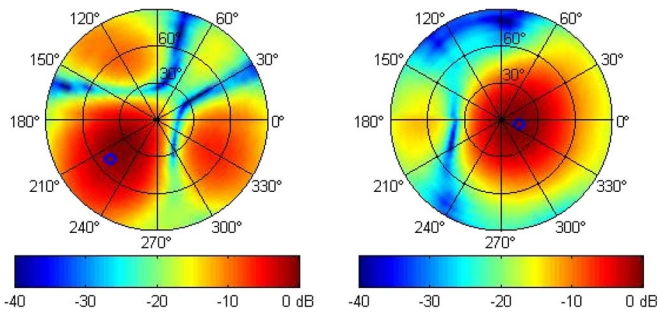


Fig. 9. Normalized power radiation patterns at 1575 MHz for right-hand circular polarization (RHCP) after adaptive beamforming for the satellites with: (left) PRN 17 and (right) PRN 27. The blue circles (in online version) indicate the corresponding DoAs of the satellite signals.

highly synchronous ADCs with a sampling rate of 104 MHz and 14-bit resolution. Due to this sub-sampling, the signal is aliased down to a lower digital IF of 26 MHz. The relation of the sampling frequency and the digital IF allows applying the so-called $fs/4$ technique to transform the signals to baseband, where fs is the sampling frequency. For the further offline signal processing, these data are filtered and down-sampled. Over a PXI interface, the recorded data is transferred to an embedded PC and stored on a 2.5-in hard disk drive. The offline processing with the DLR MATLAB software receiver is presented in [8].

D. Field Tests

In order to assess the performance of the receiver, field tests have been carried out under nearly open-sky conditions. On that occasion (August 12, 2009), the signals from nine GPS satellites could be received. Their positions in space are shown in Fig. 8, where each circle denotes the DoA of a corresponding satellite and the numbers stands for the indexes of the pseudo-random noise (PRN) ranging codes used by the satellites. The time-averaged DoA estimations obtained by using a unitary 2-D ESPRIT are indicated in Fig. 8 by the crosses. Fig. 9 presents the normalized power radiation patterns of the array antenna in the

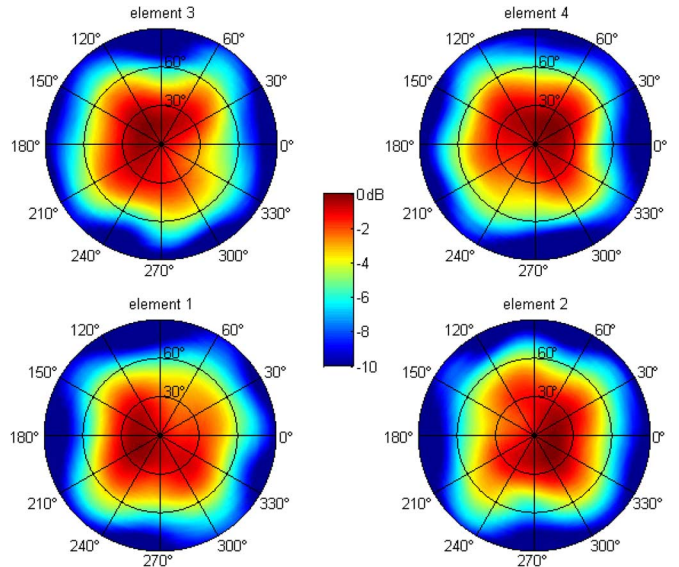


Fig. 10. Measured gain patterns of array elements at 1575 MHz for RHCP. The gain values are normalized so that the largest value around all four elements is 0 dB.

TABLE I
ERROR CHARACTERISTICS OF DoA ESTIMATION

PRN	Azimuth error (deg)		Elevation error (deg)	
	Bias	Std	Bias	Std
9	-1.85	0.40	-2.06	0.26
12	-1.95	1.21	-3.05	0.92
15	-3.21	0.40	-3.49	0.39
17	0.66	0.33	2.17	0.48
18	0.92	0.40	-2.48	0.79
22	-3.68	0.81	-12.98	1.32
26	-9.12	0.54	-2.94	0.86
27	-2.20	0.61	0.67	0.27
28	-1.36	0.47	1.53	1.22

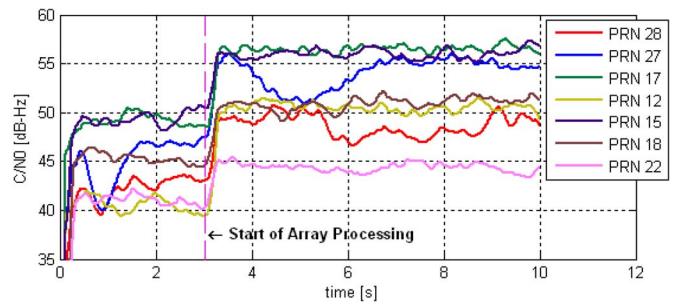


Fig. 11. Improvement of signal carrier-to-noise density ratio due to the beamforming.

complete hemisphere above the array obtained for GPS satellites with PRN 17 and PRN 27. The array weights during the test were iteratively updated with the rate of 1000 Hz using least mean squares (LMSs) algorithm and minimum mean square error (MMSE) adaptation criterion. The colors in Fig. 9 indicate the normalized power pattern in decibels according to the scales on the bottom side. The radial scale of the graphics in Figs. 8 and 9 represents the elevation angles.

Prior to these tests, the embedded radiation pattern (amplitude and phase) of each array element has been measured. All patterns have been normalized to the highest gain value between the elements (Fig. 10). They have then been used to calculate the

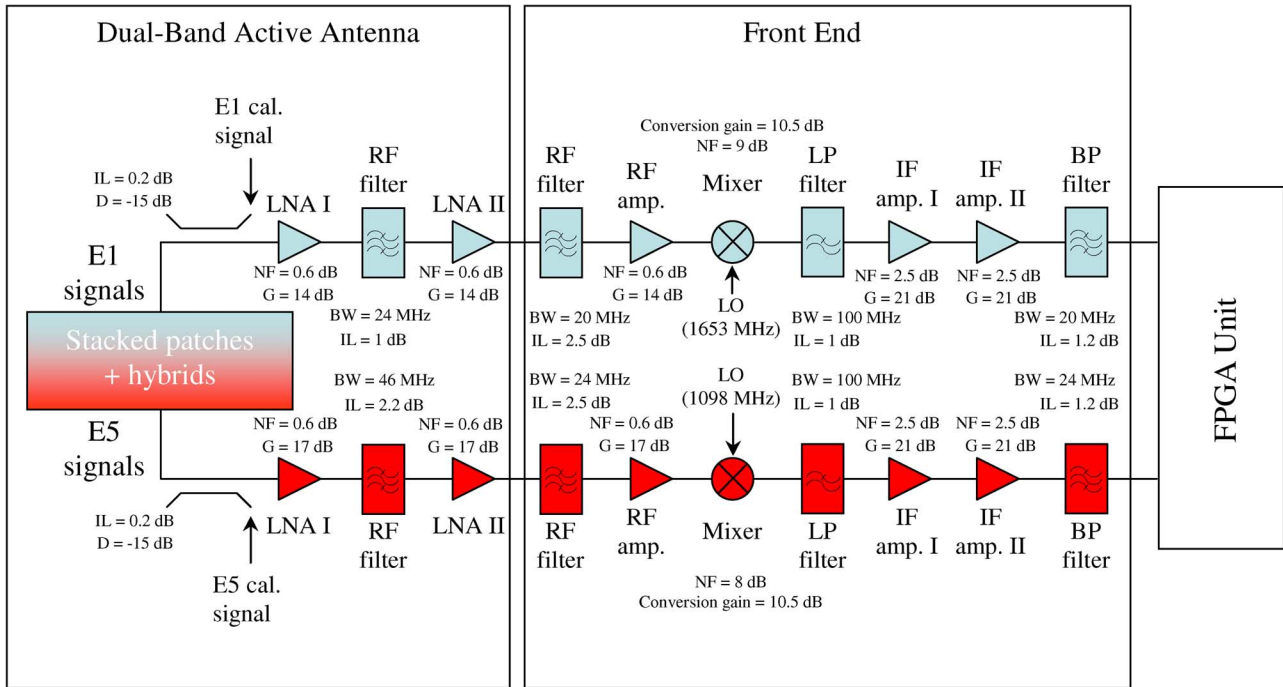


Fig. 12. Block diagram of the dual-band receiver.

radiation patterns of the entire array after beamforming (Fig. 9), as well as in the DoA estimation (Fig. 8) to improve its accuracy. Due to that, the positions of some satellites could be determined with very low error (see Table I). The largest deviation was 13° for the satellite with PRN 22 (marked in red in online version). Since the half-power beamwidth (HPBW) of the array is more than 50° , such an error in the DoA estimation does not bring about a drastic depointing loss.

The curves for the carrier-to-noise density ratio (C/N_0) as estimated by the GPS receiver before and after switching on the beamforming are shown in Fig. 11 for all visible satellites. C/N_0 is an equivalent of the signal-to-noise ratio used with spread systems. The improvement of this signal-quality measure between 3–6 dB can be observed in Fig. 11 when the receiver switches from the use of only one single antenna, the array element number 1 in Fig. 10, to the use of the entire array with the help of beamforming.

IV. DUAL-BAND RECEIVER

The robustness of GNSS receivers can be further increased by using dual-band architecture. In this case, redundancy can be achieved since the receiver can still estimate its position if interference drives the receiver into saturation in one of the two bands. Furthermore, the operation in dual-band mode allows a better estimation of the errors introduced by the ionosphere. This increases the accuracy on the position determination.

Mainly for these reasons, the third generation of the GNSS demonstrator is under development. The new concept should be able to receive and process the signals of the E5 (1.164–1.215 GHz) and E1 bands (1.559–1.591 GHz) of the European Galileo system. The E5 band is composed of E5a and E5b, which are together AltBOC modulated on a common carrier. The coherent signal processing of E5a and E5b offers

a high-positioning accuracy thanks to the large bandwidth of approx 50 MHz, but for robustness reasons, it is preferable to process E5a and E5b separately after the antenna. For safety critical applications the gain of robustness weighs more than the loss in accuracy. For that reason, the antenna was designed for the complete E5 band, whereas the frontend chains will be separated for E5a and E5b. In the current stage of development, only the E5a part of the E5 signal is used by the adjacent signal processing, but a combined E5a/E5b processing will be implemented in the next step. In order to process the signals received in the L1 and E5 band separately, a novel antenna has been designed, which allows frequency separation with high isolation without the need of a diplexer. With such an antenna, the resulting block diagram of the whole receiver is shown in Fig. 12, where the main parameters of each component have also been given. The noise figures of the E5 and E1 channels differ slightly from each other since the LNAs present 3 dB more gain in the E5 band. Nevertheless, the noise figures of each chain, from the first LNA up to its output, are estimated to be approximately 0.9 dB.

The diplexing characteristic is obtained by means of suitable impedance matching in each port of the antenna [9]. The schematic top view of the designed dual-band antenna is shown in Fig. 13. The concept is based on two stacked patches and four feed lines, where the high-frequency (HF) patch (HF patch in Fig. 13) is located in the highest level, the low-frequency (LF) patch (LF patch in Fig. 13) is between the HF patch and the ground plane containing the slots, and the feed lines are below the GND. Each of the patches resonates at a different frequency in order to obtain the dual-band characteristic. The signals received by the lower patch are coupled to the two upper right feed lines through the slots. The two lines down-left are electrically connected to the upper patch using vias. The isolation between

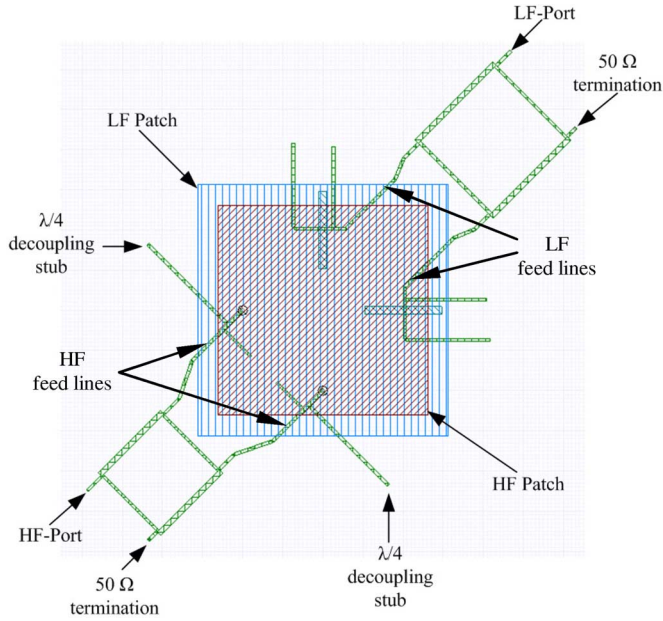
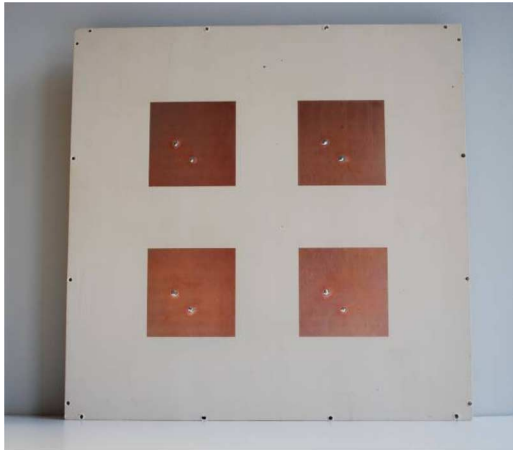


Fig. 13. Top view of the designed antenna.

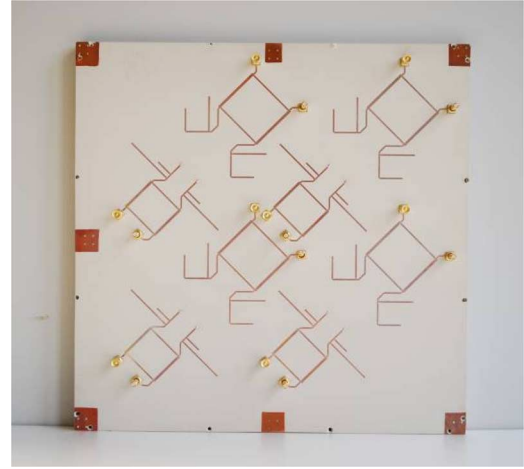
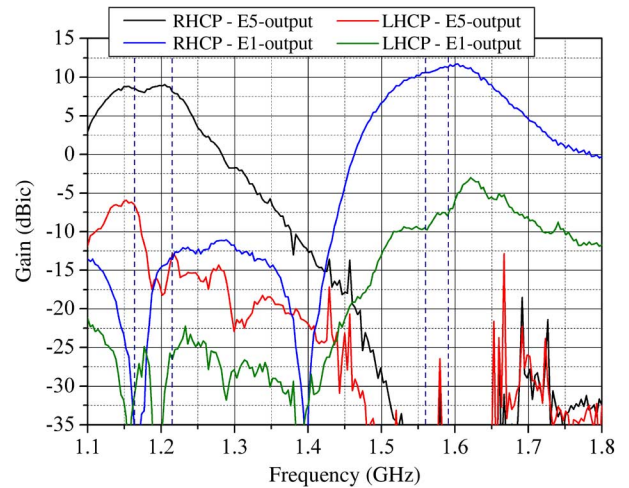
Fig. 14. Top view of the dual-band 2×2 array.

the outputs for the two different bands is achieved thanks to the two different feeding techniques plus matching networks that isolate the feeding lines exciting the fields in the same orientation (the same TM mode).

The front ends in the current stage of development are composed of independent channels for the E5a and E1 bands. Right after both outputs of each array element, directional couplers have been foreseen to couple the calibration signal into the receiver chains. The down conversion is done so that the resulting center frequency after the mixers is 78 MHz for both E5a and E1 bands.

The concept adopted for the dual-band 2×2 array follows nearly the schematic cross section shown in Fig. 3 with center-to-center interelement spacing of 90 mm. The top and bottom views of the passive part of the array are shown in Figs. 14 and 15, respectively. One can see a total of eight hybrids for the four single elements.

Due to the lack of space in the level of the hybrids, the calibration networks for both bands could not be integrated into

Fig. 15. Bottom view with the feed lines and 90° hybrids.Fig. 16. Gain curves at the LF and HF outputs of the 2×2 array.

the passive array. Therefore, these networks along with the directional couplers have been integrated in the RF board, which has been realized in multilayer technology. One calibration network has been optimized for each frequency band in stripline technology so that both are isolated one from another.

Gain measurements have been carried out for the single element and for the 2×2 array. In the broadside direction and at the central frequencies, the measured gain for the single element was 5.3 dBic. Fig. 16 shows measured results for the gain in the boresight of the 2×2 array with the elements connected by means of a broadband power divider. Isolation of at least 21.5 dB between the LF and HF outputs (blue (in online version) and black curves) has been verified. Moreover, the cross-polarization decoupling levels are at least 15.0 dB in the E5 band and 19.3 dB in the E1 band.

Although the designed single element presents nearly the same gain at both center frequencies, the resulting gain for the 2×2 array is different in the two bands. This effect is introduced by the array factor, which is frequency dependent and is given by [10]

$$AF = S_{xm}S_{yn} \quad (1)$$

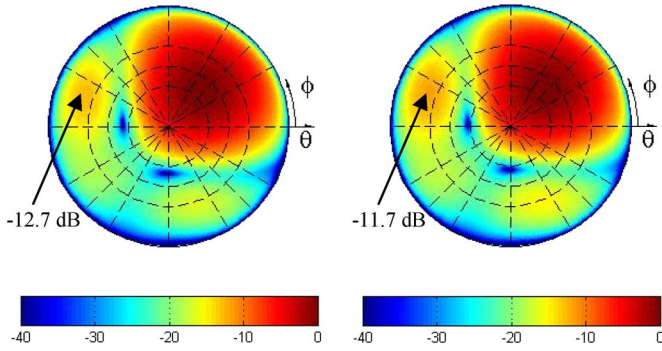


Fig. 17. Normalized power radiation patterns at 1189 MHz steered to: (left) $\theta = 70^\circ$, $\phi = 45^\circ$ and (right) $\theta = 90^\circ$, $\phi = 45^\circ$. The arrow points to the grating lobe.

where S_{xm} and S_{ym} are the array factors of linear arrays with equally spaced elements located along the x and y coordinates of a Cartesian coordinate system, respectively. For the designed array, the interelement spacing is 90 mm. Considering both central frequencies of both bands, the interelement spacing is given by $d = 0.35\lambda_{E5}$ at 1189 MHz and $d = 0.47\lambda_{E1}$ at 1575 MHz. Using this information to compute the array factor,

$$AF = 3.7 \text{ dBi at 1189 MHz}$$

and

$$AF = 6.3 \text{ dBi at 1575 MHz.}$$

For this reason, the gain of the array at both bands is different. Nevertheless, this does not represent a problem to the desired application.

Figs. 17 and 18 show simulated radiation patterns for the two central frequencies of 1189 and 1575 MHz. The array elements were excited with the same amplitude. The phases of the excitation coefficients were determined for the case of isotropic elements with the main beam steered to 45° in azimuth and 20° or 0° in elevation ($\theta = 70^\circ$ or $\theta = 90^\circ$ from the boresight). Due to nonisotropic radiation patterns and mutual coupling between the antenna elements, the achieved steering angle is smaller. For 1189 MHz and steering to $\theta = 70^\circ$ with the coefficients determined for isotropic elements, the beam points to $\theta_{\max} = 36^\circ$. Increasing the desired steering angle to $\theta = 90^\circ$ results in a very small increase of the achieved scanning angle to $\theta_{\max} = 37^\circ$ at the cost of increasing the maximal level of the grating lobes by ~ 1 dB. Therefore, the maximum scan angle of the array operating in the E5 band is 37° . Under this condition, the gain is approximately 8.2 dBic and the half-power beam width (HPBW) is 57° .

Analogously, for 1575 MHz and steering to $\theta = 70^\circ$, the maximal achieved scanning angle is $\theta_{\max} = 40^\circ$. Increasing the desired steering angle to $\theta = 90^\circ$ results in a very small increase of the achieved pointing angle to $\theta_{\max} = 41^\circ$ at the cost of increasing the level of the grating lobes by approximately ~ 1 dB. Therefore, the maximum scan angle of the array operating in the E1 band is 41° . Under this condition, the gain is approximately 9.5 dBic and the HPBW is 50° . It should be noted that the level of the grating lobes at 1189 MHz is lower than at 1575 MHz due

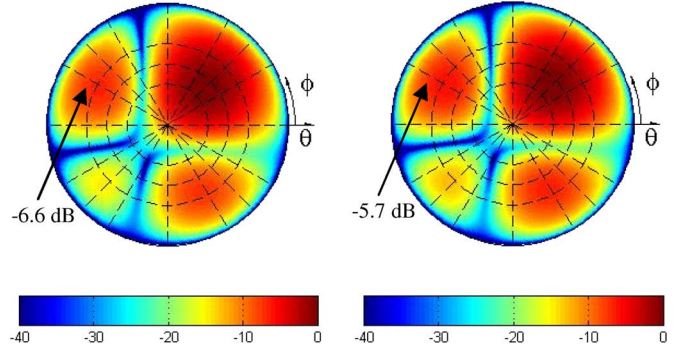


Fig. 18. Normalized power radiation patterns at 1575 MHz steered to: (left) $\theta = 70^\circ$, $\phi = 45^\circ$ and (right) $\theta = 90^\circ$, $\phi = 45^\circ$. The arrow points to the grating lobe.

to electrically smaller spacing between the antenna elements. This is also the main factor that contributes to the fact that the maximum scanning angle in the E1 band is larger than for E5 band.

Although the proposed 2×2 planar array cannot be steered to very low elevations, it can still receive signals from low elevations (lower than 8°) with positive gain. This does not represent a limitation of the designed receiver since the signals coming from very low elevations (typically lower than 10°) should be rejected for most of the SoL applications so as to reduce the reception of multipath and interference produced by on-ground sources.

V. CONCLUSION

The concepts and implementation issues of three different technology demonstrators for GNSS systems that have been developed at the DLR have been discussed in this paper. Field tests have been carried out with the single-band system, where the performance of the receiver, DoA, and DBF algorithms could be tested. Results for the estimation of the satellite position in space showed that good predictions have been obtained.

The concept of the dual-band GNSS receiver has also been described. Measured results of gain in the boresight direction indicate that the antenna presents high isolation between the two outputs. This is an interesting property that may be employed not only for navigation systems, but also in several other applications where dual-band technology is required. Moreover, this approach allows designing the RF chain for each frequency band independently right after the antenna, thus simplifying the design process of the whole receiver system.

Although the goals of the presented demonstrators were the design and the implementation of navigation receivers composed of 2×2 arrays, the presented technology is not limited to this array size. Increasing the number of array elements would surely increase system complexity, but it would also bring improvements in the system robustness. One of the benefits of a receiver employing a larger antenna array is that a larger number of interferers may be suppressed. The tradeoff between performance and system complexity seems to be the main point that has to be analyzed when developing innovative SoL navigation receivers.

REFERENCES

- [1] M. V. T. Heckler, M. Cuntz, A. Konovaltsev, L. A. Greda, A. Dreher, and M. Meurer, "Development of robust safety-of-life navigation receivers at the german aerospace center (DLR)," in *IEEE MTT-S Int. Microw. Symp. Dig.*, Anaheim, CA, CA, May 2010, pp. 85–88.
- [2] M. Cuntz, H. Denks, A. Konovaltsev, A. Hornbostel, E. Schittler-Neves, A. Dreher, and M. Meurer, "A GNSS prototyping platform with digital beamforming capabilities for sol applications," in *Toulouse Space Show/Eur. Navigat. Conf.*, Toulouse, France, Apr. 2008, [CD ROM].
- [3] E. S. Neves, P. de Vita, and A. Dreher, "Modular smart antenna array for GPS and Galileo applications," in *Eur. Navigat. Conf.*, Munich, Germany, Jul. 2005, [CD ROM].
- [4] E. S. Neves, M. V. T. Heckler, A. A. Selga, and A. Dreher, "Beamforming analysis on a broadband antenna array for the galileo system," in *IEEE Int. AP-S Symp.*, Albuquerque, NM, Jul. 2006, pp. 1129–1132.
- [5] M. V. T. Heckler, W. Elmarissi, L. A. Greda, M. Cuntz, and A. Dreher, "Narrow-band microstrip antenna array for a robust receiver for navigation applications," in *3rd Eur. Antennas Propag. Conf.*, Berlin, Germany, Mar. 2009, pp. 1206–1210.
- [6] "Interim minimum operational performance specification for airborne equipment, version 0.25," EUROCAE, Malakoff, France, Oct. 2007.
- [7] "Minimum operational performance standards for global positioning system/wide area augmentation system airborne equipment," RTCA, Washington, DC, DO 229D, Feb. 2006.
- [8] A. Konovaltsev, F. Antreich, and A. Hornbostel, "Performance assessment of antenna array algorithms for multipath and interferers mitigation," presented at the 2nd GNSS Signals and Signal Processing Workshop, Noordwijk, The Netherlands, Apr. 24–25, 2007.
- [9] M. V. T. Heckler, E. N. Lavado, and A. Dreher, "Dual-band circularly polarized microstrip antenna with two isolated outputs suitable for navigation systems," in *IEEE AP-S Int. Symp.*, Charleston, SC, Jun. 2009, [CD ROM].
- [10] C. A. Balanis, *Antenna Theory: Analysis and Design*, 2nd ed. New York: Wiley, 1997.



Marcos V. T. Heckler (M'06) was born in Rio Grande, Brazil, in 1978. He received the B.Sc. degree in electrical engineering (with an emphasis in electronics) from the Universidade Federal de Santa Maria (UFSM), Santa Maria, Brazil, in 2001, the M.Sc. degree in electronic engineering (microwaves and optoelectronics) from the Instituto Tecnológico de Aeronáutica (ITA), São José dos Campos, Brazil, in 2003, and the Dr.-Ing. degree in electrical engineering from the Technische Universität München, Munich, Germany, in 2010.

From April to August 2003, he was a Research Assistant with the Antennas and Propagation Laboratory, ITA. From October 2003 to June 2010, while working toward the doctoral degree, he was a Research Associate with the Antenna Group, Institute of Communications and Navigation, German Aerospace Center (DLR). He is currently an Assistant Professor with the Universidade Federal do Pampa, Alegrete, Brazil. His current research interests are the design of microstrip antennas and arrays and the development of numerical techniques for conformal microstrip antennas.



Manuel Cuntz received the Diploma degree in electrical engineering from the Technical University of Kaiserslautern, Kaiserslautern, Germany, in 2005.

In 2006, he joined the Institute of Communications and Navigation, Institute of Communications and Navigation, German Aerospace Center (DLR), Wessling, Germany. His research interest is multi-antenna satellite navigation receivers.



Andriy Konovaltsev received the Engineer diploma and Ph.D. degree in electrical engineering from the Kharkov State Technical University of Radio Electronics, Kharkov, Ukraine, in 1993 and 1996, respectively.

Since 2001, he has been with the Institute of Communications and Navigation of the German Aerospace Center (DLR), Wessling, Germany, where he is currently a Research Associate. His research interests are array processing for satellite navigation systems, signal processing algorithms including synchronization, and multipath and radio

interference mitigation.



Lukasz A. Greda (M'01) received the Dipl.-Ing. (M.S.) degree from the Technical University, Kielce, Poland, in 1999, and the Dr.-Ing. (Ph.D.) degree from FernUniversität, Hagen, Germany, in 2005, both in electrical engineering.

From 1999 to 2004, he was a Research Assistant with the Department of Electrical Engineering, FernUniversität. Since 2004, he has been with the Institute of Communications and Navigation, German Aerospace Center (DLR), Wessling, Germany, as a Research Assistant with the Antenna Research Group. His current research interests include the analysis of microstrip antennas, smart antennas, and antenna technology for satellite communications and navigation.



Achim Dreher (M'92–SM'99) received the Dipl.-Ing. (M.S.) degree from the Technische Universität Braunschweig, Braunschweig, Germany, in 1983, and the Dr.-Ing. (Ph.D.) degree from FernUniversität, Hagen, Germany, in 1992, both in electrical engineering.

From 1983 to 1985, he was a Development Engineer with Rohde & Schwarz GmbH and Company KG, Munich, Germany. From 1985 to 1992, he was a Research Assistant, and from 1992 to 1997, he was a Senior Research Engineer with the Department of Electrical Engineering, FernUniversität. Since 1997, he has been with the Institute of Communications and Navigation, German Aerospace Center (DLR), Wessling, Germany, where he is currently Head of the Antenna Research Group. He is a Scientific Coordinator and permanent Lecturer for the Carl Cranz Series for Scientific Education in the area of smart antenna systems. His current research interests include analytical and numerical techniques for conformal antennas and microwave structures, smart antennas for satellite communications and navigation, and antenna technology for radar applications.

Dr. Dreher is a member of the VDE/ITG Expert Committee on Antennas.



Michael Meurer (S'98–A'03–M'04–SM'05) received the Diploma and Ph.D. degrees in electrical engineering from the University of Kaiserslautern, Kaiserslautern, Germany.

Upon graduation in 1998, he joined the Research Group for Radio Communications, University of Kaiserslautern, as a Research Engineer and then as a Senior Key Researcher and Senior Lecturer. Since 2005, he has been an Associate Professor (Priv-Doz.) with the Technical University of Kaiserslautern.

Moreover, since 2006, he has been with the German Aerospace Center (DLR), Institute for Communications and Navigation, Wessling, Germany, where he is the Director of the Department for Navigation and the Coordinating Director of the DLR Centre of Excellence for Satellite Navigation. He has authored or coauthored four books/book chapters and over 100 technical papers. He has invented or holds over 25 patents.

Dr. Meurer is a member of international expert and advisory groups, including the European Commission's Compatibility, Signal and Interoperability Working Group (formerly known as the Galileo Signal Task Force). He was the recipient of several awards.